Geomechanics and Engineering, *Vol. 39, No. 5 (2024) 513-528*
https://doi.org/10.12989/gae.2024.39.5.513

The role of dynamic compaction method in mitigating the seismic vulnerability of liquefiable sites using fragility functions: A case study

Mahdieh Afshari[1a] and Hamid Alielahi*[2]

[1]*Department of Civil Engineering, University of Science and Culture, Tehran, Iran*
[2]*Department of Civil Engineering, Zanjan Branch, Islamic Azad University, Zanjan, Iran*

(*Received March 22, 2024, Revised November 11, 2024, Accepted November 19, 2024*)

Abstract. The soil layers in the site of Pars Service Port (PSP) have significant risks of liquefaction due to seismic activity. In order to mitigate the liquefaction hazards, Dynamic Compaction (DC) method as a cost-effective solution has been employed. Hence, by comparing a probabilistic assessment of liquefaction hazards before and after DC at PSP using fragility functions, the effectiveness of DC in the reduction of liquefaction hazards can be quantified. In fact, the fragility analysis and assessment for liquefiable sites have not been paid enough attention to. This study focuses on the liquefaction possibility of PSP at the seismic levels through liquefaction risk maps before and after DC. Risk maps play a crucial role in determining land use and reducing the vulnerability of structures and sites. Examining the liquefaction risk maps of PSP enables proactive measures to prevent the construction of high-importance structures in areas with a moderate, high, or severe exceedance probability of liquefaction. This approach helps to avoid potential risks and ensures that construction projects are carried out in safer locations.

Keywords: dynamic compaction; fragility curves; liquefaction potential index; risk map; seismic vulnerability

1. Introduction

Earthquake damage can occur in two main forms: direct and indirect. One form of direct earthquake damage leads to soil liquefaction (New Zealand geotechnical society 2016). Liquefaction typically leads to various forms of damage, including land subsidence, lateral spreading, etc. Studies conducted by Shen *et al.* (2019a) have reported extensive damage caused by liquefaction, affecting buildings, infrastructure, and port facilities. Considering this, the evaluation of liquefaction in ports holds great importance in the field of geotechnical engineering regarding the significant role ports play as crucial commercial and economic links for every country during earthquakes, the likelihood of liquefaction is notably high in ports due to the presence of loose and saturated soils. In fact, liquefaction can lead to significant damage in port areas (Rabeti Moghadam *et al.* 2017).

Analysis of liquefaction risk in each region can be evaluated in either qualitative, quantitative or even both approaches (Meslem *et al.* 2021). In quantitative analysis, safety factor (FS_{liq}) and liquefaction potential index (LPI) are used (Robertson and Wride 1998, Moss *et al.* 2006, Khoshnevisan *et al.* 2015, Hicks 2018, sonmezer and Korkmaz 2023), while for qualitative analysis, the liquefaction severity indices such as low, moderate, high, or very high are used. Iwasaki *et al*. (1984) presented the damage threshold limit of the LPI in both quantitative and qualitative approaches so that for LPI < 5, low liquefaction, 5 < LPI < 15, high liquefaction, and for LPI > 15, very high liquefaction is observed. By evaluating quantitative and qualitative LPI values, microzonation maps can be presented in each area as these maps have been used to examine the risk of liquefiable sites, which is one of the most challenging issues today. It is important to note that calculating the liquefaction potential of sites requires in-situ tests. However, these tests are not entirely reliable; for example, the Cone Penetration Test (CPT), while widely used, carries some uncertainties when applied to liquefied sites. Previous research has taken specific measures to minimize these uncertainties (Guan and Wang 2024, Yang *et al.* 2023). By analyzing the resistance of soil against moderate to severe levels of liquefaction-induced damage, these maps provide essential information for decision-making processes, especially in determining suitable locations for structures with high importance class and minimizing the potential risks as well as enhancing overall safety and resilience. Also, these maps have played a key role in selecting more stable sites for urban planning and management and reducing economic costs (Lai *et al.* 2021, Bozzoni *et al.* 2021). In providing liquefaction risk maps, it is essential to apply globally recognized guidelines and regulations. So, in this study, the regulations presented by the New Zealand Geotechnical Society (NZGS) and Ministry of Business Innovation and Employment (MBIE) guidelines (2016) are adopted.

This study demonstrates the impact of soil remediation through the DC method using analytical fragility curves and presents the results in the form of PSP risk maps. In 2023, a research study was conducted in the Kalyani region of India to assess liquefaction potential. The investigation involved

*Corresponding author, Associate Professor
E-mail: ha.alielahi@iau.ac.ir
[a]MSc.
E-mail: mahdiehaf2010@gmail.com

ISSN: 2005-307X (Print), 2092-6219 (Online)

evaluating liquefaction potential in six selected boreholes using the method proposed by Iwasaki *et al.* (1984). The research aimed to mitigate probable damages by generating risk maps in liquefiable areas (Kumar *et al.* 2023). According to existing evidence and previous studies, the implementation of the DC method has shown positive effects on enhancing the performance of land in mitigating the risk of liquefaction during past earthquakes liquefaction (Lee *et al.* 2001, Hausler and Koelling 2004, Shenthan *et al.* 2004, Michalowski and Nadukfuru 2012, Shen *et al.* 2019b).

Given the findings of prior studies, it is evident that there has been a scarcity of research dedicated to exploring the seismic vulnerability of liquefiable sites and the impact of soil remediation on them, particularly with the aid of fragility curves in different damage states with probability distribution estimates of explanatory parameters. Notably, the predominant focus in existing literature has been on deriving fragility curves for sites influenced by liquefaction. Among the limited studies conducted in this field, some scholars have developed fragility curves to predict the liquefaction consequences with empirical, logistic regression, Bayesian network, or other methods (Ge *et al.* 2023, Geyin and Maurer 2020, Meng *et al.* 2023).

The primary objective of this study is to assess the vulnerability of the liquefiable site of PSP through analytical fragility curves and to explore the efficacy of soil remediation using the DC method in mitigating seismic hazards. Seismic fragility curves serve as a tool to depict potential structural conditions encountering or surpassing specific failure limits across various ground motion scenarios, measured by earthquake intensity measures (IMs) like PGA or PGV. Essentially, fragility curves express the probability of exceeding defined performance states at different damage levels for diverse earthquake intensities, encapsulating uncertainties in both structural capacity and demand. Consequently, leveraging fragility curves enables the anticipation of potential structural damage, facilitating informed decisions regarding appropriate repair or strengthening measures for structures and sites. Moreover, fragility curves play a crucial role in assessing the risk to urban infrastructure. These curves provide insights into the expected damage levels at different earthquake intensities.

This multi-dimensional approach provides a deeper and more nuanced understanding of vulnerability and risk. While previous studies have recognized the impacts of liquefiable sites, their primary focus has typically been on the fragility of infrastructure and building structures. As a result, the thorough assessment of liquefaction probabilities under varying earthquake intensities has often been inadequate. By utilizing fragility curves to identify structural vulnerabilities, prioritization for remediation efforts becomes more informed. A pivotal aspect of this research lies in assessing seismic vulnerability at the PSP site through the application of a less commonly explored yet robust method for determining the safety factor against liquefaction, as proposed by Idriss and Boulanger (2014).

The safety factor against liquefaction (FS_{liq}) serves as an input for calculating the LPI (Maurer *et al.* 2015, Sonmez 2003), followed by the generation of fragility curves based on these indices. This comprehensive approach involves a series of procedural steps for constructing fragility curves and evaluating the impact of DC remediation on mitigating seismic vulnerability across various levels of damage. The study aims to achieve these objectives through the application of analytical fragility curves, ultimately presenting liquefaction probability results in the form of microzonation maps.

Fig. 1 Geographical location of PSP

Fig. 2 Aerial image of PSP

2. Pars Service Port (PSP) description

The pars service port, located along the Persian Gulf coast between longitudes 52°30'41" to 52°34'21" East and latitudes 27°25'51" to 27°32'13" North, stands 270 km southeast of Bushehr port. With ten heavy wharf posts, it efficiently handles diverse cargo, including containers, dry bulk, liquid bulk, and heavy goods (Figs. 1 and 2). Additionally, the port plays a crucial role in servicing wellhead platforms of floating gas condensate export terminals like Single Buoy Mooring (SBM) and providing marine services for the export of petrochemical products at the adjacent Pars Petrochemical Port. This study focuses on the PSP, established to harness the gas reserves of the South Pars basin and drive industrial and economic activities in oil, gas, petrochemical, and downstream petrochemical industries. The Pars port complex encompasses two key components: Pars Petrochemical and Service Ports. The PSP holds particular significance due to its extensive range of assigned activities within the entire Pars Special

Fig. 3 The hinterland exploitation area

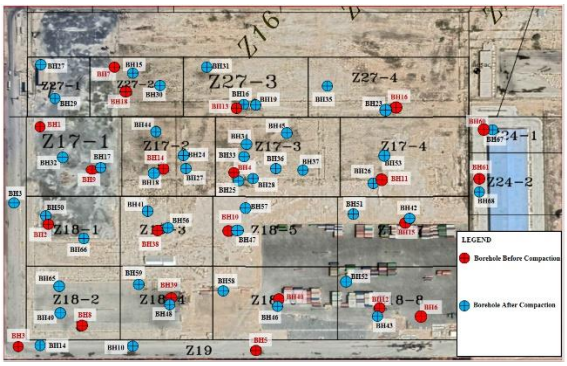

Fig. 4 Location of drilled boreholes in the investigated zones of liquefaction before and after of DC

Economic Energy Zone. Fig. 2 provides an overview of the Pars service port, while Fig. 3 depicts the exploitation area of this port.

2.1 Geotechnical conditions of the region

The hinterland of the port is composed of sea-dredged materials, typically silty sand or silty sandy gravel with relatively low to moderate relative compaction. The underground water level in the port area is approximately 1.5 meters deep. Comprehensive geological and geotechnical studies, including field and laboratory tests, have been conducted to understand the exploitation layers of the PSP land. The results, including the Standard Penetration Test (SPT), indicate that the exploitation areas have loose and settling soil (seed *et al.* 1985). Therefore, soil remediation in these areas is crucial, and the Dynamic Compaction (DC) method emerges as an appropriate and cost-effective solution for soil improvement. In certain areas, where no significant structures were present and based on engineering judgments, boreholes were not drilled, considering the natural soil type and usage requirements. In areas where drilling occurred, high Standard Penetration Test (SPT) numbers (50 and above) indicated strong soil with no liquefaction concerns. The selection of zones 17, 18, 19, 24, and 27 for liquefaction assessment and subsequent soil remediation using the DC method was guided by factors like ground type, soil compaction, land use, and specific soil operations needed.

Zones 17, 18, 19, and 24 were identified as having soft soil, making them more susceptible to liquefaction. Conversely, zone 27, with hard soil, exhibited greater

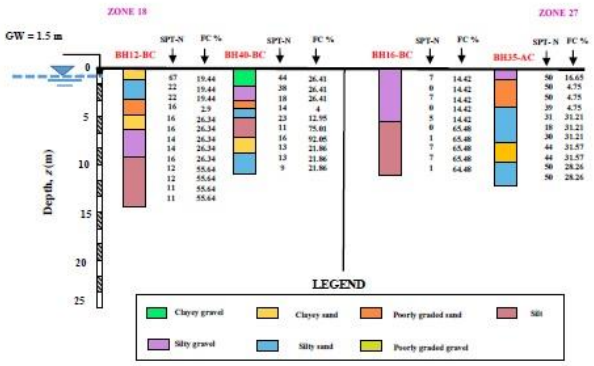

Fig. 5 An example of soil profile based on drilled boreholes

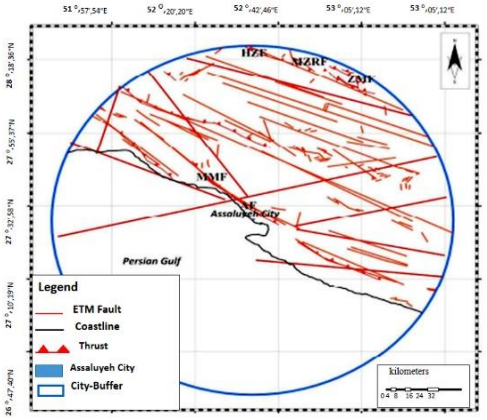

Fig. 6 Tectonic map in Asalouye site

resistance to liquefaction. Fig. 4 illustrates boreholes before and after remediation, with a total of 67 boreholes drilled in the land, 22 before soil remediation, and 45 after DC remediation. Additionally, Fig. 5 presents an example of the soil profile based on the drilled boreholes.

2.2 Seismic conditions of the region

Seismic hazard analysis in a region can be undertaken through two primary approaches: deterministic and probabilistic. In contrast to the deterministic method, which relies on models or discrete single-value events to assess seismic risk, the probabilistic approach incorporates multiple values or continuous events. In the initial phase of risk analysis, seismic sources capable of influencing the targeted scenario are identified. In risk analysis, a seismic zone is conceptualized as a combination of probabilities, whether in the form of points, lines, or surfaces (Sonmez and Korkmaz 2023). Within these zones, earthquakes are presumed to occur at a consistent rate concerning their size or magnitude. In this study, the International Institute of Earthquake Engineering and Seismology (IIEES) employed a probabilistic approach for the Asalouyeh site. Fig. 6 illustrates the earthquake-producing faults in the Asalouyeh region as identified in seismicity studies.

Generally, in order to design port structures through the performance-based design approach, considering the varying importance levels of structures, different seismic levels are taken into account. For each seismic level, the

permissible amount of damage is determined. In this particular port, the assessment of soil liquefaction potential focuses on two seismic levels, labeled as level 1 and level 2. Level 1 corresponds to an earthquake with a 50% likelihood of occurring over the structure's useful life, possessing a return period of 75 years. Conversely, level 2 signifies an earthquake with a 10% chance of occurrence during the structure's useful life, carrying a return period of 475 years (PIANC 2001, Alielahi and Nadernia 2022).

Based on the seismic hazard study in this region, the first level corresponds to a PGA of 0.23 g, with M_w = 6.5, and the second level corresponds to a PGA of 0.42 g, with M_w = 7.1.

3. Liquefaction assessment of Pars Service Port (PSP) site

The combination of a high-water level and seismic activity in the area makes lands developed using hydraulic embankment methods, such as the container area of PSP, highly susceptible to liquefaction. To assess liquefaction risk and vulnerability in this region, SPT field test data, the method proposed by Idriss and Boulanger (2014) and potential indices developed by Maurer *et al.* (2015) and Sonmez (2003) are employed. Fragility curves are used to investigate the probability of liquefaction occurrence and assess vulnerability levels before and after implementing remediation measures, specifically focusing on the effects of DC in mitigating liquefaction hazards in the targeted liquefiable site. The study's outcomes are presented through liquefaction risk maps.

3.1 Investigation of soil liquefaction by I&B method

To evaluate soil liquefaction during earthquakes, the methods proposed by Idriss and Boulanger (2014) are employed in this study. These methods offer a semi-experimental approach and provide practical relationships that can be applied in real-world scenarios. Specifically, the simplified method introduced by Seed and Idriss (1971) is used to estimate cyclic stress ratio (CSR), which represents the ground movement-induced stress during an earthquake, as shown in Eq. (1). In Eq. (2), a modification is made by incorporating rd, which is determined based on M and z (Idriss and Boulanger 2008, 2014). Additionally, Eq. (5) represents the cyclic resistance ratio (CRR) used in the calculations. Notably, when evaluating the CRR, the influence of fine particles in the standard penetration test number ($(N_1)_{60}$) is taken into account, as indicated by Eqs. (6) and (7).

$$\mathrm{CSR} = 0.65(r_d)(a_{max}/g)(\sigma_v/\sigma'_{vo})(1/\mathrm{MSF})(1/K_\sigma) \quad (1)$$

$$r_d = exp[\alpha(z) + \beta(z)\,M] \quad (2)$$

$$\begin{cases} \alpha(z) = -1.012 - 1.126\ sin\left(\dfrac{z}{11.73} + 5.133\right) \\ \beta(z) = 0.106 + 0.118\ sin\left(\dfrac{z}{11.28} + 5.142\right) \end{cases} \quad (3)$$

where z is up to a maximum depth of 20 meters.

The MSF in Eq. (1) is related to the moment magnitude M and can be rewritten as (Idriss and Boulanger 2014)

$$MSF = 6.9.exp\left(\frac{-M}{4}\right) - 0.058 \le 1.8 \quad (4)$$

$$CRR = exp\left[\frac{(N_1)_{60cs}}{14.1} + \left(\frac{(N_1)_{60cs}}{126}\right)^2 - \left(\frac{(N_1)_{60cs}}{23.6}\right)^3 + \left(\frac{(N_1)_{60cs}}{25.4}\right)^4 - 2.8\right] \quad (5)$$

$$(N_1)_{60_{CS}} = (N_1)_{60} + \Delta(N_1)_{60} \quad (6)$$

where $\Delta(N_1)_{60}$ is equal to

$$\Delta(N_1)_{60} = \exp[1.63 + (9.7/FC + 0.01) - (15.7/FC + 0.01)^2] \quad (7)$$

In the final stage of the analysis, the possibility of liquefaction in the region was assessed using the safety factor (FS_{liq}), calculated as the ratio of *CRR* to *CSR*, as expressed in Eq. (8). Following the Seismic Guidelines of Japanese Ports, the safety factor was evaluated against specific thresholds. A FS_{liq} below 1.5 for level 1 and below 1 for level 2 of design earthquakes suggests a potential for liquefaction in the area (PIANC 2001, OCDI 2020).

$$FS_{liq} = \frac{CRR}{CSR} \quad (8)$$

3.2 Investigation of liquefaction potential index

In this research, the liquefaction classification by Sonmez (2003), which is an update of Iwasaki et al.'s method (1978), and Maurer *et al*.'s method (2015), which is a modified version of Ishihara's approach (1985), have been employed. Eqs. (9) and (12) pertain to Sonmez and Maurer *et al*., respectively. The results of LPI calculations from the modified Ishihara method by Maurer *et al*. are presented with the abbreviation ISH. The LPI is calculated through Eq. (9) by the Sonmez method.

$$LPI = \int_0^{20m} F(FS_{liq}) \times w(z)dz \quad (9)$$

where

$$F(FS_{liq}) = \begin{cases} 1 - FS_{liq} & ; \ FS_{liq} \le 0.95 \\ 0 & ; \ FS_{liq} \ge 1.2 \\ 2 \times 10^6 \times e^{-18.427 FS_{liq}} & ; \ 0.95 < FS_{liq} < 1.2 \end{cases} \quad (10)$$

$$w(z) = 10 - 0.5z \quad (11)$$

FS_{liq} is calculated from Eq. (8) by the method of Idriss a nd Boulanger (2014). Also, w(z) is a function of the depth o f soil layers (z) in meters.

$$\mathrm{LPI_{ISH}} = \int_{H_1}^{20\mathrm{m}} F(\mathrm{FS_{liq}}) \times w(z)\mathrm{dz} \quad (12)$$

$$w(z) = \frac{25.56}{z} \quad (13)$$

$$F(FS_{liq}) = \begin{cases} 1 - FS_{liq} & ; \ FS_{liq} \le 1 \ and \ H_1 \times m(FS_{liq}) \le 3 \\ 0 & ; \ Otherwise \end{cases} \quad (14)$$

Fig. 7 Soil remediation of PSP by DC method

Table 1 Sonmez division of LPI (2023)

Liquefaction potential index (LPI)	Severity class of liquefaction
Non-liquefiable	LPI = 0
Low	0 < LPI ≤ 2
Moderate	2 < LPI ≤ 5
High	5 < LPI ≤ 15
Very high	LPI >15

$$m(FS_{liq}) = exp\left(\frac{5}{25.56(1 - FS_{liq})}\right) - 1 \quad (15)$$

In Eq. (14), H_1 is based on the criterion of Ishihara (1985).

Sonmez's (2003) division has been used for the LPI criterion according to Table 1 in this study.

4. Soil remediation method in site of Pars Service Port (PSP)

Given the loose layers and soil liquefaction depth in PSP, the DC method has been implemented as potentially the most suitable approach for soil remediation in the region. DC operations are conducted experimentally in liquefaction-prone areas of the PSP, as illustrated in Fig. 7.

The first step in this experimental design is to choose the weight and drop height to achieve the desired effective depth, using Eq. (16). The empirical coefficient is set between 0.35 and 0.5, based on soil permeability in each region. Additionally, a sufficient amount of energy (AE) must be applied during DC, evaluated using Eq. (17) (Lukas 1995). Four compaction patterns (A, B, C, and D) are then designed as per the guidelines.

$$D = n\sqrt{WH} \quad (16)$$

$$AE = \frac{N.W.H.P}{S^2} \quad (17)$$

Specifically, pattern B is implemented for zone 17, and pattern A for zones 24 and 27, with the remediation depth considered as 7 meters in these three zones according to the geotechnical soil conditions. In zones 18 (pattern C) and 19 (pattern D), the remediation depth was specifically addressed, with a depth of 15 meters being considered. This information is visualized in Figs. 8 and 9. Additionally,

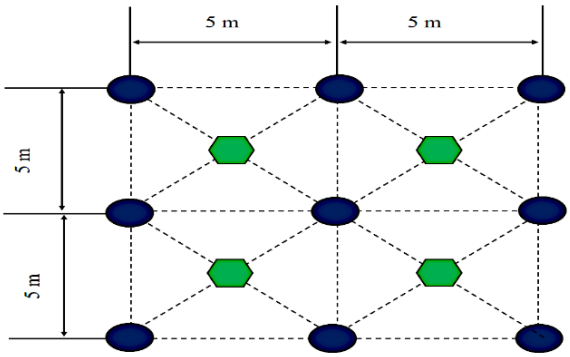

Fig. 8 Patterns A and B of DC

Table 2 Calculated parameters in two sections of pattern A

Type A pattern	Compaction stage	Number of compactions	Sign	W (tons)	H (m)	Applied energy	S (m)	n
	First stage	7	⬢	20	20	300 $\frac{kJ}{m^3}$	5	0.35
	Second stage	7	●	20	20	300 $\frac{kJ}{m^3}$	5	0.35
	Third stage	Ironing	-	7	3	-	Adjacent to each other	-

Table 3 Calculated parameters in two sections of pattern B

Type A pattern	Compaction stage	Number of compactions	Sign	W (tons)	H (m)	Applied energy	S (m)	n
	First stage	10	⬢	15	13	250 $\frac{kJ}{m^3}$	5	0. 5
	Second stage	10	●	15	13	250 $\frac{kJ}{m^3}$	5	0. 5
	Third stage	Ironing	-	7	3	-	Adjacent to each other	-

Tables 2 to 5 provide the pertinent parameters associated with the compaction patterns utilized in the study.

Table 4 Calculated parameters in two sections of pattern C

	Number of passes	Compaction stage	Number of compactions	Sign	W (tons)	H (m)	Applied energy	S (m)	n
Type C pattern	First pass	First stage	10	⬢	35	15	$250\frac{kJ}{m^3}$	10	0.5
		Second stage	8	●	35	15	$250\frac{kJ}{m^3}$	10	0.5
	Second pass	First stage	10	■	20	15	$250\frac{kJ}{m^3}$	5	0.5
		Second stage	8	▲	20	15	$250\frac{kJ}{m^3}$	5	0.5
	-	Third stage	Ironing	-	7	3	-	Adjacent to each other	-

Table 5 Calculated parameters in two sections of pattern D

	Number of passes	Compaction stage	Number of compactions	Sign	W (tons)	H (m)	Applied energy	S (m)	n
Type C pattern	First pass	First stage	10	⬢	35	25	$300\frac{kJ}{m^3}$	10	0.35
		Second stage	8	●	35	25	$300\frac{kJ}{m^3}$	10	0.35
	Second pass	First stage	8	■	28	18	$300\frac{kJ}{m^3}$	5	0.35
		Second stage	6	▲	28	18	$300\frac{kJ}{m^3}$	5	0.35
	-	Third stage	Ironing	-	7	3	-	Adjacent to each other	-

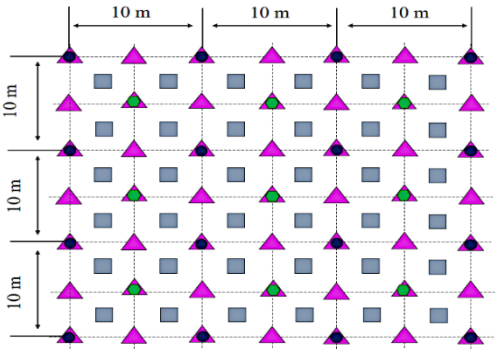

Fig. 9 Patterns C and D of DC

Safety factor diagrams for various boreholes in PSP at different soil depths have been generated in accordance with Fig. 10. Utilizing the relationships outlined in Section (3.1), these diagrams are constructed for seismic level 2, considering a PGA of 0.42 g, which represents a more critical safety factor range. The analysis is conducted for zones 17, 18, 19, 24, and 27. Before remediation, Fig. 10(a) illustrates that the safety factor values of boreholes up to a depth of 15 meters are predominantly below one in most instances. Following remediation, depicted in Fig. 10(b), the liquefaction safety factor values for the same boreholes have risen above one, signifying the positive impact of the remediation efforts in the service port.

Following the implementation of the DC method, the LPI of vulnerable areas has been re-examined using the methods mentioned in section (3.2) on the seismic level 2 with the PGA of 0.42g. Figs. 11 and 12 depict liquefaction maps before and after the DC intervention in PSP. These maps are prepared based on the criteria established by Maurer *et al*. (2015) and Sonmez (2003) at seismic level 2.

The categorization in these maps is according to Sonmez LPI, classified into five categories: non-liquefaction, low liquefaction, moderate liquefaction, high liquefaction, and very high liquefaction, as outlined in Table 1.

The positive effect of DC in the specified areas is clearly demonstrated (Figs. 12(a) and 12(b)). Before remediation, the LPI values in most zones fell within the high-intensity class, ranging from 5 < LPI < 15 (Figs. 11(a) and 11(b)). However, post-remediation, the LPI values have shifted to the moderate class, with 2 < LPI < 5, and even further to the low class, with 0 < LPI < 2 (Figs. 12(a) and 12 (b)). This shift signifies a notable reduction in liquefaction potential, showcasing the effectiveness of the remediation process.

5. Developing fragility curves

Fragility curves express the possible conditions of the encountering or exceedance of a structure or site from a specific damage limit according to different parameters such as Peak Ground Acceleration (PGA), peak ground displacement (PGD), peak ground velocity (PGV), spectral acceleration (Sa), etc. In general, there are different methods for producing fragility curves, including experimental, engineering judgment, analytical, and combined methods (Alielahi and Rabeti Moghadam 2017).

Fragility curves are drawn by the analytical method in this study. These curves represent a function of probabilities (P) and are characterized by various distribution functions. Typically, for drawing fragility curves, the Gaussian curve or ϕ as shown in Fig. 13 is employed. This curve exhibits a bell-shaped pattern, commonly utilized in fragility curve construction (Elnashai and Di Sarno 2008, Zheng *et al*. 2023). These distribution curves have random variables on the horizontal axis and each variable has a median and standard deviation, and their distribution function is

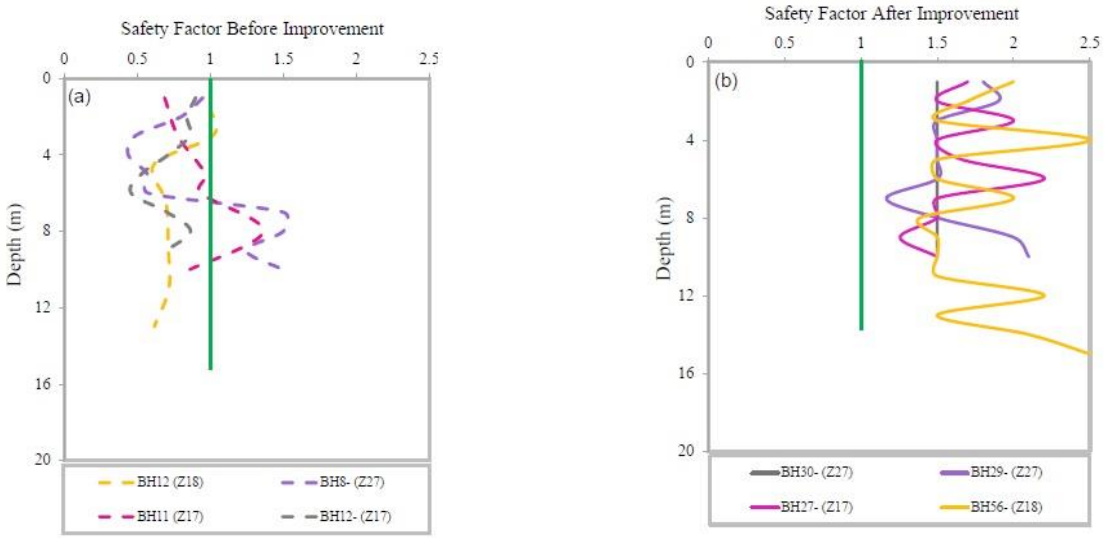

(a) Before DC (b) After DC

Fig. 10 The safety factor of liquefaction of boreholes drilled with the PGA = 0.42 g (Idriss and Boulanger 2014

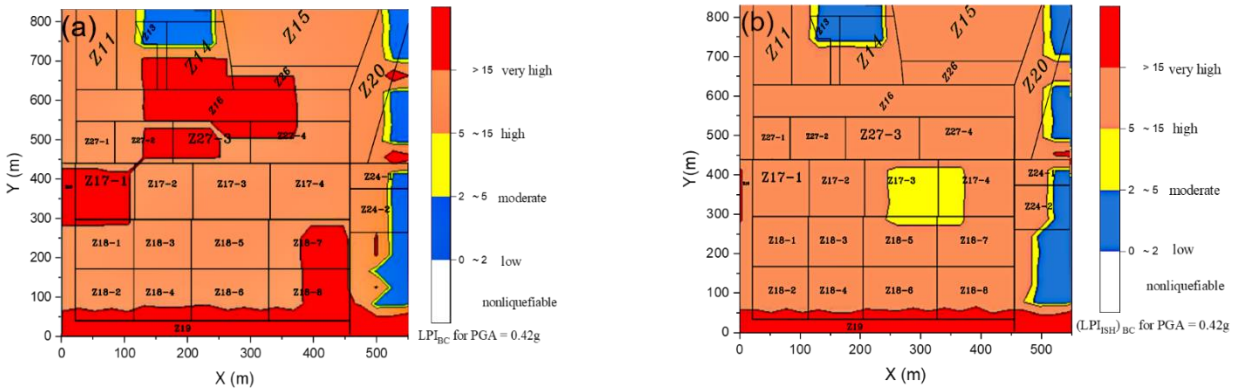

(a) based on Maurer *et al.* (2015) (b) based on Sonmez (2003)

Fig. 11 LPI of PSP zones before the remediation of DC

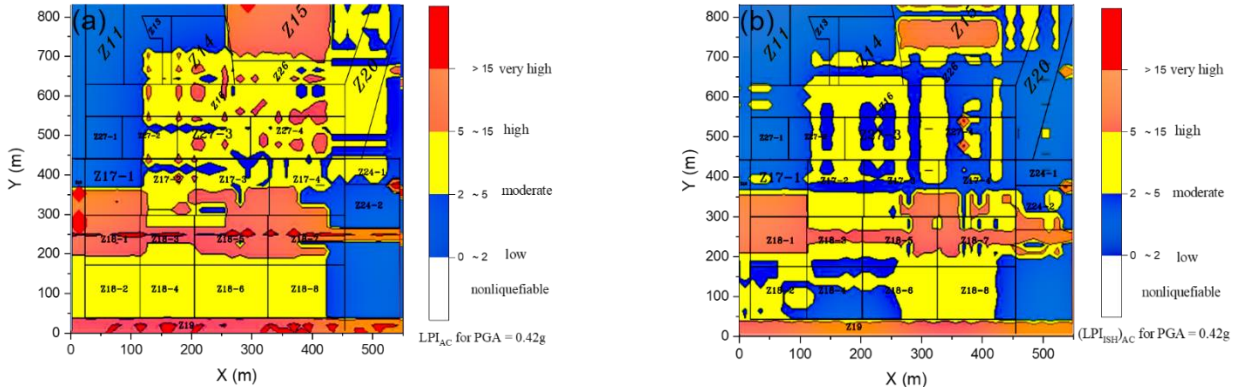

(a) based on Maurer *et al.* (2015) (b) based on Sonmez (2003)

Fig. 12 LPI of PSP zones after the remediation of DC

expressed by Eq. (18). In this equation, x represents the random variable distributed logarithmically (ln(x)) (Porter 2021, Ilbagitaher and Alielahi 2024). To calculate the probability value of a normal distribution, the cumulative distribution function is employed, visualized as the surface area under the normal curve, as depicted in Fig. 14. The function of the cumulative distribution is described by Eq. (19) (Elnashai and Di Sarno 2008). Fragility functions are defined according to Eqs. (20) and (21). In Eq. (21), ln (*LPI*(*AC*)) is the limit state of damage due to liquefaction,

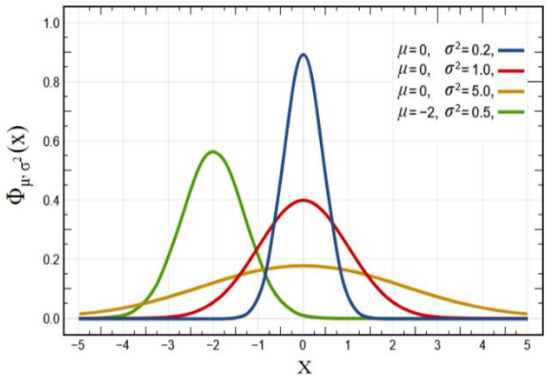

Fig. 13 Normal distribution diagram in various mean and standard deviation (Elnashai and Di Sarno 2008)

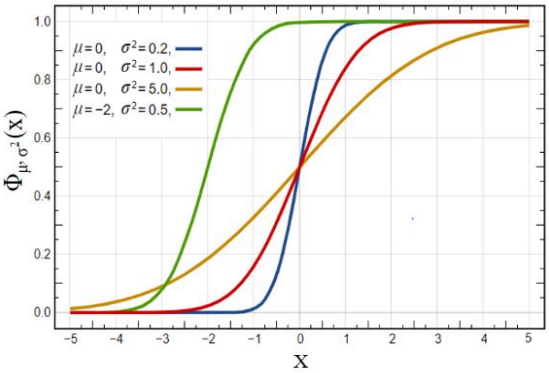

Fig. 14 Cumulative normal distribution diagram in various mean and standard deviation (Elnashai and Di Sarno 2008)

which is equal to the random variable of this study ln (*LPI*(*AC*)) = ln (*x*). *EPD* is an engineering demand parameter and has a unique statistical distribution in the fragility curves at any point of earthquake intensity. In the service port, the liquefaction potential index values were used as engineering demand (*EPD* = *LPI*), which was obtained according to Eqs. (9) and (12) and Table 1 in Section (3.2). The intensity measure (*IM*) serves as the parameter indicating the intensity of external phenomena, such as PGA, PGV, etc., during an earthquake. In this study, the intensity parameter selected is the peak ground acceleration (PGA), considered at six different levels ranging from 0.1 g to 1 g (0.1 g, 0.2 g, 0.4 g, 0.6 g, 0.8 g, and 1 g). In the construction of fragility curves, the X-axis represents the *IM* value, and the Y-axis signifies the probability percentage of structural damage based on the engineering demand parameter (Khanbabazadeh *et al.* 2022). Additionally, *AC*, denoting acceptable conditions based on assumed limit states from the New Zealand Code, is considered. In this study, various damage levels were determined using the LPI and liquefaction safety factor in the fragility curves, aligning with Table 6 of the New Zealand Code.

According to the regulations of New Zealand, damage levels are categorized into six categories (L0-L5). In the fragility curves developed for the PSP, four levels (L2-L4) of these regulations are utilized. L2 represents a moderate damage level, L3 corresponds to a high damage level, and

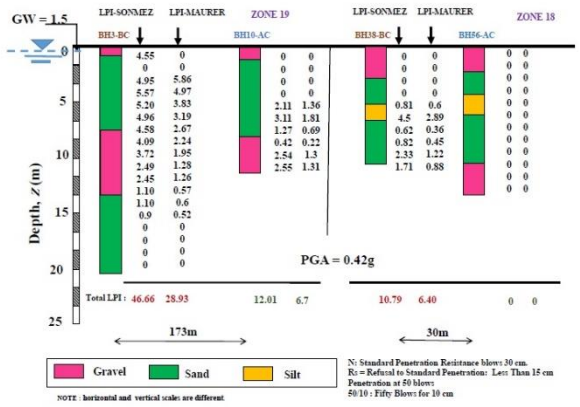

Fig. 15 LPI diagram of selected boreholes based on Sonmez (2003) and Maurer *et al*. (2015) criteria with the PGA = 0.42 g

L4 indicates a severe damage level (Table 6). The parameters λ and ξ in the fragility curves are derived from the median (μ) and standard deviation (σ) of a normal distribution, as specified in Eq. (22) (Haldar and Mahadevan 2000).

$$F_x(x) = \frac{1}{\sigma\sqrt{2\pi}} e^{-\frac{(x-\mu)^2}{2\sigma^2}} \tag{18}$$

$$F_x(x) = \frac{1}{\sigma\sqrt{2\pi}} \int_0^{x_1} e^{-\frac{(x-\mu)^2}{2\sigma^2}} dx = \phi\left(\frac{x-\mu}{\sigma}\right) \tag{19}$$

$$Fragility = P[EPD > AC \mid IM] \tag{20}$$

$$P = P[EPD > AC] = 1 - P[EPD < AC] = 1 - \phi\left(\frac{ln(LPI(AC)) - \lambda}{\xi}\right) \tag{21}$$

$$\xi^2 = \ln\left(1 + \frac{\sigma^2}{\mu^2}\right) ; \lambda = \ln\mu - \frac{1}{2}\xi^2 \tag{22}$$

6. Results and discussion

Based on the methodology outlined in the previous sections, the liquefaction potential in each borehole is determined according to the criteria of Sonmez (2003) and Maurer *et al.* (2015) at PGA values of 0.23 g (seismic level 1) and 0.42 g (seismic level 2). The calculations are performed both before and after the implementation of DC, and the results of some selected boreholes are summarized in Table 7.

According to Table 7, the LPI values before remediation based on the Sonmez (2003) criterion and Maurer *et al.* (2015) criterion, in majority of zones during an earthquake with a PGA of 0.42 g were in high class and after remediation, these values decreased. This significant reduction in liquefaction potential clearly demonstrates the positive effects of DC in mitigating the risk of liquefaction in the service port zones.

Also, based on Fig. 15, the liquefaction diagrams of selected boreholes in zones 18 and 19 demonstrate the effect of DC remediation on reducing the risk of

Table 6 Classification of damage levels due to liquefaction according to the LPI and the safety factor of the New Zealand regulation (New Zealand Geotechnical Society 2016)

Characteristic FL, LPI	Characteristics of liquefaction and its consequences	Effects from excess pore water pressure and liquefaction	Performance Level
L0	Insignificant	No significant excess pore water pressures (no liquefaction).	FL > 1.4; LPI=0; LSN <10
L1	Mild	Limited excess pore water pressures; negligible deformation of the ground and small settlements	FL > 1.2; LPI = 0; LSN = 5 – 15
L2	Moderate	Liquefaction occurs in layers of limited thickness (small proportion of the deposit, say 10 percent or less) and lateral extent; ground deformation results relatively small in differential settlements	FL ≈ 1.0; LPI < 5; LSN 10 – 25
L3	High	Liquefaction occurs in a significant portion of the deposit (say 30 percent to 50 percent) resulting in transient lateral displacements, moderate differential movements, and settlement of the ground in the order of 100 mm to 200 mm	FL < 1.0; LPI = 5 – 15; LSN = 15 – 35
L4	Severe	Complete liquefaction develops in most of the deposit resulting in large lateral displacements of the ground, excessive differential settlements, and a total settlement of over 200 mm	FL << 1.0; LPI > 15; LSN > 30
L5	Very severe	Liquefaction resulting in lateral spreading (flow), large permanent lateral ground displacements and/or significant ground distortion (lateral strains/stretch, vertical offsets and angular distortion).	-

Table 7 LPI values of boreholes based on Sonmez (2003) and Maurer *et al*. (2015) criteria in PSP zones before and after DC

Boreholes	LPI BC (0.23g)		LPI BC (0.42g)		Name of Boreholes	LPI AC (0.23g)		LPI AC (0.42g)	
	LPI	LPIISH	LPI	LPIISH		LPI	LPIISH	LPI	LPIISH
BH6	0.000	0.000	0.000	0.000	BH50	0.980	0.400	9.430	5.230
BH8	1.280	0.660	11.440	5.970	BH66	0.000	0.000	10.030	5.490
BH2	0.020	0.000	17.390	10.970	BH49	0.000	0.000	3.050	2.720
BH39	0.080	0.000	9.640	6.120	BH65	0.000	0.000	2.200	1.170
BH10	0.000	0.000	5.420	3.130	BH59	0.240	0.130	3.760	2.050
BH38	2.220	1.430	10.790	6.400	BH48	0.000	0.000	3.740	1.930
BH40	0.940	0.610	14.970	10.640	BH57	0.000	0.000	0.760	0.390
BH12	0.000	0.000	19.410	12.340	BH47	0.320	0.320	14.290	8.590
BH15	0.760	0.460	15.540	10.420	BH41	0.000	0.000	6.510	4.130
BH9	0.000	0.000	7.600	6.440	BH56	0.000	0.000	0.000	0.000
BH1	3.380	2.160	13.890	9.850	BH46	0.000	0.000	2.600	1.630
BH14	1.450	0.760	17.260	14.150	BH58	0.000	0.000	4.620	2.410
BH4	0.250	0.000	19.420	12.930	BH43	0.000	0.000	0.000	0.000
BH11	0.000	0.000	9.660	7.370	BH52	0.000	0.000	0.000	0.000
BH5	9.350	6.040	32.890	20.660	BH51	0.000	0.000	0.150	0.000
BH3	19.500	13.640	45.660	28.930	BH42	0.000	0.000	5.450	8.020
BH60	0.030	0.000	18.050	10.520	BH17	0.000	0.000	0.570	0.300
BH61	1.420	1.020	25.890	18.670	BH32	0.000	0.000	0.000	0.000
BH16	0.000	0.000	8.570	7.580	BH44	0.000	0.000	2.800	2.070
BH13	2.620	2.620	15.550	13.890	BH18	0.000	0.000	5.950	4.730
BH18	0.000	0.000	2.190	0.000	BH24	0.000	0.000	2.110	1.320
BH7	0.000	0.000	0.380	0.000	BH27	0.000	0.000	0.000	0.000

liquefaction. In zone 18, the LPI values of the borehole (BH38-BC) before remediation and (BH56-AC) after remediation are shown. In zone 19, the LPI values of the borehole (BH3-BC) before remediation and (BH10-AC) after remediation are shown. The comparison clearly indicates the positive effect of DC remediation in reducing the risk of liquefaction, as evident from the lower LPI values after the remediation process.

In Figs. 16 and 17, fragility curves before and after DC for the liquefaction potential indices of Sonmez (2003) and

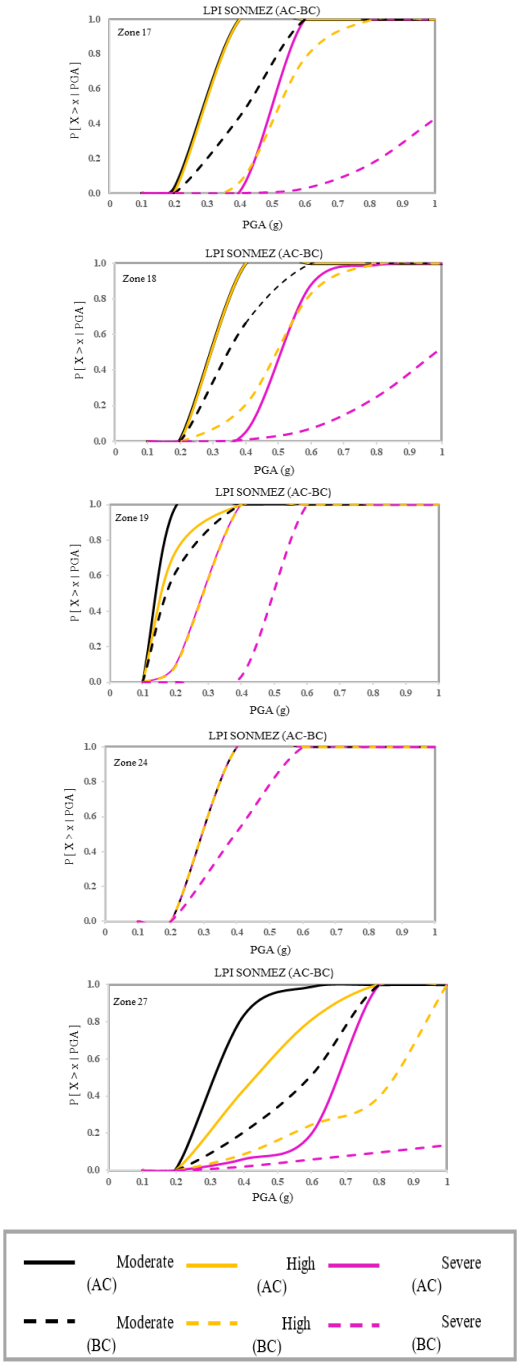

Fig. 16 Fragility curves before and after DC at PGA of 0.1 g to 1 g for zones 17, 18, 19, 24, and 27 based on the LPI of Sonmez (2003)

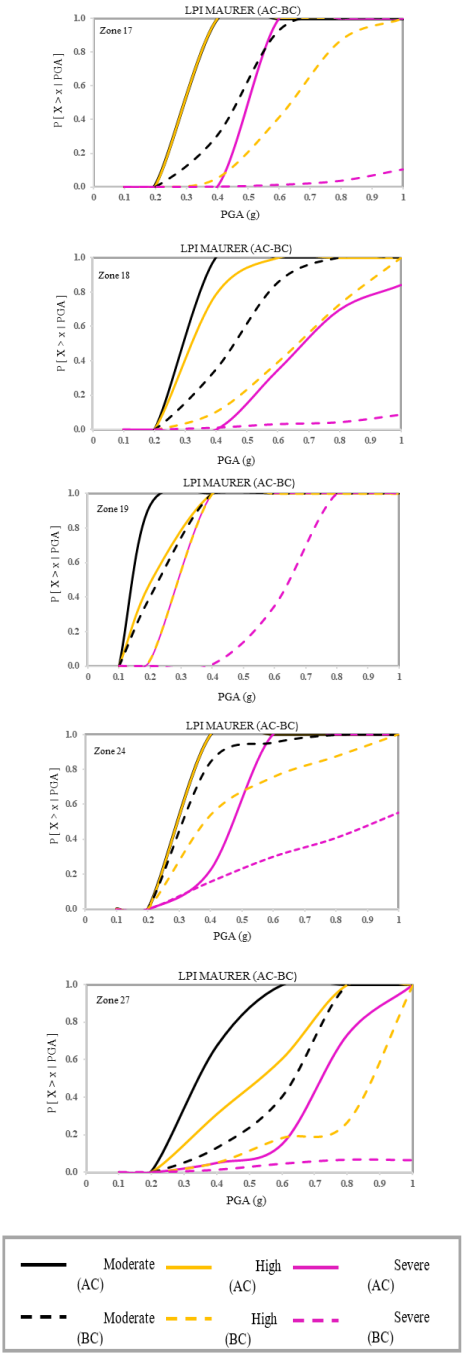

Fig. 17 Fragility curves before and after DC at PGA of 0.1 g to 1 g for zones 17, 18, 19, 24, and 27 based on the LPI of Maurer *et al*. (2015)

Maurer *et al.* (2015) have been presented to assess the vulnerability of PSP at different levels of liquefaction-induced damage. The fragility curves allow estimating the probability of liquefaction risk ($P(LPI)$) based on the liquefaction potential index (LPI) in zones 17, 18, 19, 24, and 27. The analytical fragility curves provide the probability percentages of site vulnerability to liquefaction in three damage levels: moderate, high, and severe, according Table 6 (New Zealand geotechnical society 2016).

These probabilities for seismic points at level one and level two are extracted from the curves and presented in Tables 8 and 9, respectively. In the fragility curves, the probability of liquefaction risk is depicted for three damage levels: moderate, high, and severe. The curves represent the probabilities before remediation as solid lines and after remediation as dashed lines. For instance, based on Sonmez's potential index the curve of zone 27 at a seismic level of PGA = 0.42 g, the probabilities of site vulnerability before remediation are as follows: 5% for severe damage,

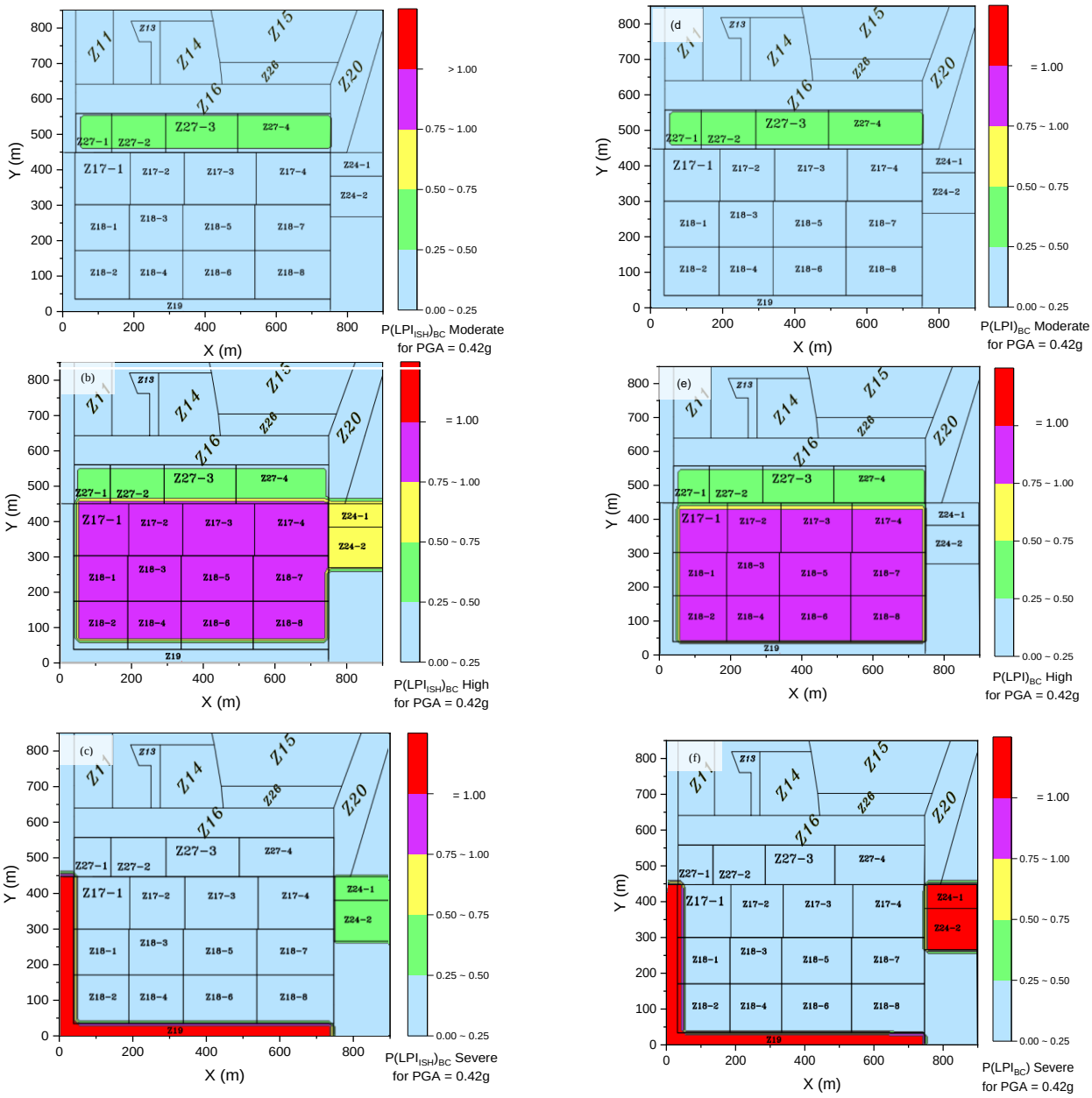

Fig. 18 Maps of the probability of vulnerability of PSP to liquefaction at the seismic level two (PGA=0.42 g) before DC on the three damage levels; a, b, and c) related to Sonmez's potential index (2003); d, e, and f) related to Maurer *et al.*'s (2015) potential index.

43% for high damage, and 44% for moderate damage. After remediation, these probabilities decrease to 2% for severe damage, 7% for high damage, and 16% for moderate damage. The probability of no damage before remediation (P =1-P) is 8%, while after remediation, the probability of no damage significantly increases to 75% (Fig. 16).

Based on Maurer *et al.*'s potential index in the curve of zone 27, before remediation at PGA = 0.42 g, the probabilities of vulnerability are 5% for very high damage, 33% for high damage, and 40% for moderate damage. After remediation, these probabilities decrease to 1% for very high damage, 5% for high damage, and 12% for moderate damage. The probability of no damage (*P =1-P*) is 22% before remediation, while after remediation, the probability of no damage increases to 82% (Fig. 17).

For each of zones 17, 18, 19, 24, and 27, which were prone to liquefaction, a fragility curve was drawn, and the total of fragility curves were presented before remediation and other curves were drawn for after remediation, half of which is based on the potential index of Sonmez (2003) and the other half is based on the index of Maurer *et al.* (2015). According to Figs. 18 and 19, the values in three damage level (Moderate, High, Severe) are obtained by fragility curves. It should be noted that after drawing the curves at the seismic level 1, the probability of site vulnerability of the service port against liquefaction in the three damage

Table 8 Investigating the probability of liquefaction in three damage levels based on Sonmez's (2003) criteria and New Zealand regulations (2016)

damage levels	zone	P(LPI) Before Compaction (BC)		P(LPI) After Compaction (AC)	
		0.23 g	0.42 g	0.23 g	0.42 g
Moderate	Z17	0.02	0	0	0.4
	Z18	0	0	0	0.51
	Z19	0.25	0	0.62	0
	Z24	0	0	0	0
	Z27	0.01	0.44	0	0.16
High	Z17	0	0.82	0	0.19
	Z18	0	0.82	0	0.27
	Z19	0.73	0	0	0.82
	Z24	0	0	0	0.38
	Z27	0	0.43	0	0.07
Severe	Z17	0	0.18	0	0
	Z18	0	0.18	0	0.01
	Z19	0.1	1	0	0.18
	Z24	0.03	1	0	0.62
	Z27	0	0.05	0	0.02

Table 9 Investigating the probability of liquefaction in three damage levels based on Maurer *et al.*'s (2015) criteria and New Zealand regulations (2016)

damage levels	zone	P(LPI) Before Compaction (BC)		P(LPI) After Compaction (AC)	
		0.23 g	0.42 g	0.23 g	0.42 g
Moderate	Z17	0.01	0	0	0.32
	Z18	0	0.12	0	0.24
	Z19	0.45	0	0.4	0
	Z24	0	0	0	0.32
	Z27	0	0.40	0	0.12
High	Z17	0.02	0.88	0	0.08
	Z18	0	0.84	0	0.17
	Z19	0.45	0	0	0.96
	Z24	0	0.68	0	0.40
	Z27	0	0.33	0	0.05
Severe	Z17	0	0.12	0	0
	Z18	0	0.04	0	0.01
	Z19	0.03	1	0	0.04
	Z24	0	0.32	0	0.18
	Z27	0.01	0.05	0	0.01

levels before the remediation according to Tables 8 and 9 is very small, therefore, the site of the service port will be safe against an earthquake with a magnitude of M_w = 7.1 and PGA = 0.23 g and will not undergo liquefaction.

The vulnerability maps of PSP are categorized into 5 parts, each represented by a distinct color. The color scheme is as follows: blue signifies the probability of liquefaction events in damage levels (moderate, high, severe) from 0-25%, green from 25-50%, yellow from 50-75%, purple from 75-100%, and red in 100%. These maps visually illustrate changes in the probability of site vulnerability before and after DC. For example, at the high level of damage according to Maurer et al.'s index (2015), areas that were originally purple (75-100% vulnerability) have transformed into blue (0-25%), indicating a substantial reduction in vulnerability at the high damage level. In the Sonmez index (2003) at the high level of damage, areas previously purple have shifted to green and blue, showcasing decreased vulnerability. Furthermore, the probability of vulnerability in Zones 19 and 24 was 100% at the very high damage level, and after remediation, it has decreased to 18% in Zone 19 and 64% in Zone 18.

7. Conclusions

This research focused on assessing the vulnerability of the area of PSP to liquefaction across various damage levels (low, moderate, high, and severe) using the LPI of Maurer *et al*. (2015) and Sonmez (2003) in conjunction with fragility curves. The outcomes were presented through liquefaction risk microzonation maps. Based on the LPI values obtained, it was determined that during an earthquake with a magnitude of M_w = 6.5 and a PGA = 0.23 g (corresponding to seismic level 1), PSP is considered safe, and significant damage from liquefaction is not observed. However, under more severe seismic conditions with a magnitude of M_w = 7.1 and a PGA = 0.42 g (corresponding to seismic level 2 with), it is recommended to implement appropriate measures to mitigate potential damages caused by liquefaction. The remediation approach of DC has demonstrated positive effects in reducing the risk of liquefaction at the Pars service port site, as indicated by the results and outputs from the liquefaction risk maps. Before remediation, the probability of liquefaction at high and severe levels of damage was generally between 75-100% in most zones. However, after remediation, the range of liquefaction damage has significantly decreased to 0-25% in these zones. It is essential to note that in certain areas of the site, the probability of vulnerability due to DC may not have changed significantly. This could indicate the uncertainty associated with the effectiveness of DC as a remediation method. To address this, it may be beneficial to explore and implement different compaction patterns tailored to each LPI. The results obtained from the liquefaction risk microzonation maps based on the two different liquefaction potential indices (Maurer *et al*. 2015, and Sonmez 2003) are generally consistent with each other. However, it is noted that in some areas, the maps based on the Sonmez LPI values tend to be more conservative, indicating a higher level of estimated liquefaction risk. Indeed, fragility curves play a crucial role in assessing the vulnerability of a site and selecting appropriate design criteria for structures based on their importance. They provide valuable information on the probability of exceeding a certain damage level for different levels of ground-shaking intensity. Consequently, these curves could be applied to predict the probability of liquefaction occurrence at different seismic levels in the future. It is important to recognize that the methodology employed in

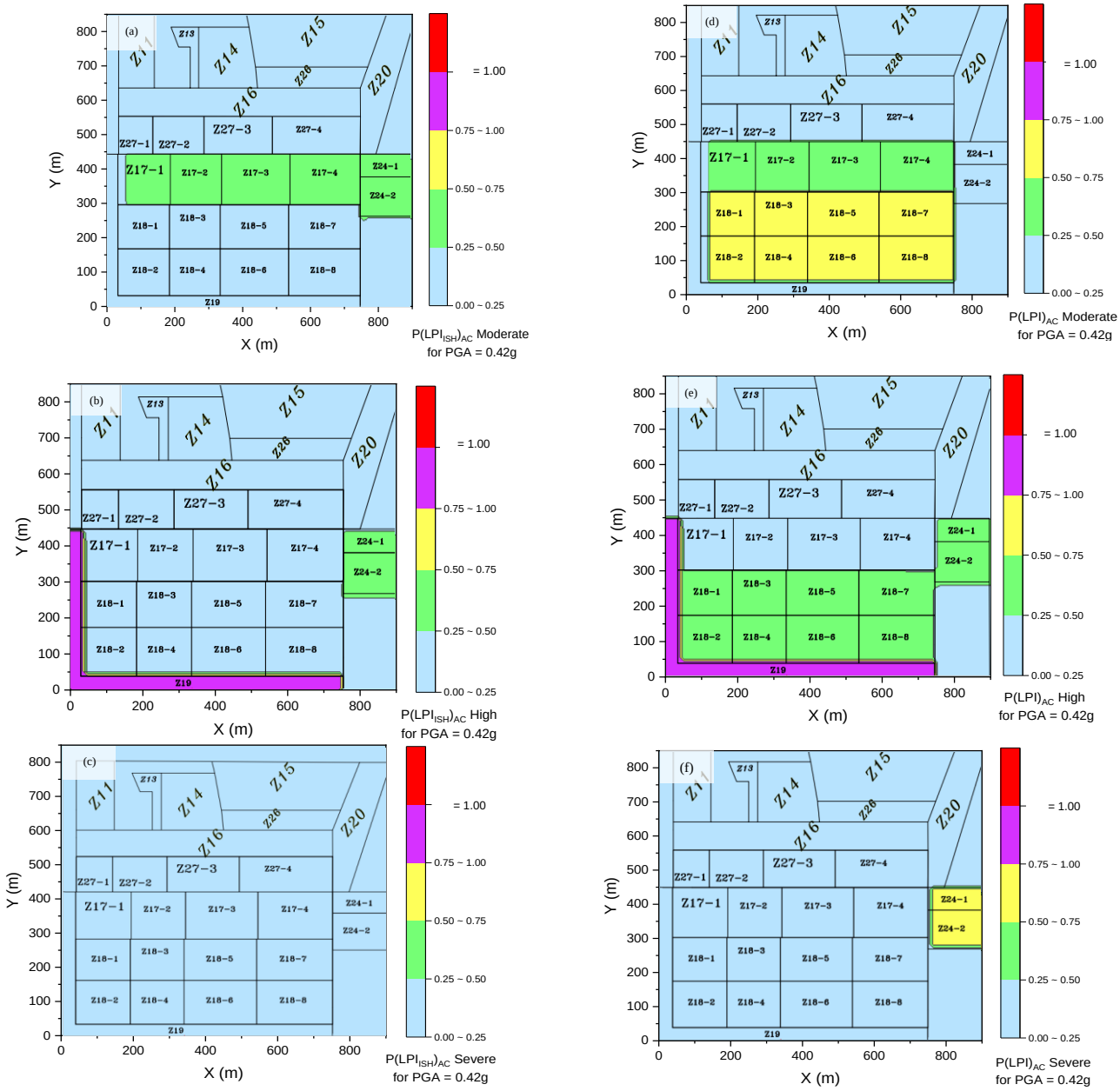

Fig. 19 Maps of the probability of vulnerability of PSP to liquefaction at the seismic level two (PGA=0.42 g) after DC on three damage levels; a, b, and c) related to Sonmez's potential index (2003); d, e, and f) related to Maurer *et al.*'s (2015) potential index.

this study is specific to the research conducted and should be further validated and examined in future studies with different site specifications and conditions. Each site has its unique geological and geotechnical characteristics, which can influence the liquefaction behavior and the effectiveness of remediation methods. Therefore, it is recommended to adapt and verify the results, formulas, and fragility functions obtained in this study for other projects and regions. Future research endeavors should focus on refining and enhancing the methodologies used to mitigate the risk associated with liquefaction-prone sites. This can involve exploring alternative remediation techniques, incorporating additional site-specific parameters, and considering a wider range of ground motion scenarios.

Acknowledgments

The authors hereby appreciate the Sahel Iranian Consulting Engineers and Mr. Danyal Yahyapour for providing information relevant to this study. Also, the authors would like to express their great thanks to Mr. Ali Derakhshan for his valuable assistance in editing the manuscript.

References

Alielahi, H. and Nadernia, Z. (2022), "The study on yield acceleration and permanent displacement of broken-back gravity quay walls – a case study", *Mar. Georesour. Geotec.*, **40**(11), 1275-1288. https://doi.org/10.1080/1064119X.2021.1988008.

Alielahi, H. and Rabeti Moghadam, M. (2017), "Fragility curves evaluation for broken-back block quay walls", *J. Earthq. Eng.*, **21**(1), 1-22. https://doi.org/10.1080/13632469.2016.1142487.

Boulanger, R.W. and Idriss I.M. (2014), *CPT And SPT Based Liquefaction Triggering Procedures*. Rep. No. UCD/CGM-14/01. Center for Geotechnical Modeling Department of Civil and Environmental Engineering University of California, Davis, California, USA.

Bozzoni, F., Bonì, R., Conca, D., Lai, C.G., Zuccolo, E. and Meisina, C. (2021), "Megazonation of earthquake-induced soil liquefaction hazard in continental Europe", *Bull. Earthq. Eng.*, **19**(10), 4059-4082. https://doi.org/10.1007/s10518-020-01008-6.

Eberhard, M.O., *et al*. (2010), "The mw 7.0 Haiti earthquake of January 12, 2010, USGS/EERI advance reconnaissance team report. US Geological Survey Open-File Report 2010-1048", 1-58.

Elnashai, A.S. and Di Sarno, L. (2008), *Fundamentals of Earthquake Engineering: from source to fragility*, 2nd Ed., John Wiley & Sons, https://doi.org/10.1002/9780470024867.

Ge, Yi., Zhang, Z., Zhang, J. and Huang, H, (2023), "Developing region-specific fragility function for predicting probability of liquefaction induced ground failure", *Probab. Eng. Mech.*, **71**(103381), 1-10. https://doi.org/10.1016/j.probengmech.2022.103381.

Geyin, M. and Maurer, B.W. (2020), "Fragility functions for liquefaction-induced ground failure", *J. Geotech. Geoenviron. Eng.*, **146**(12), 04020142-14. https://doi.org/10.1061/(ASCE)GT.1943-5606.0002416.

Guan, Z. and Wang, Y. (2024), "Risk-informed adaptive sampling strategy for liquefaction severity mapping", *Georisk: Assessment and Management of Risk for Engineered Systems and Geohazards,* **18**(2), 526-539. https://doi.org/10.1080/17499518.2023.2225165.

Haldar., A. and Mahadevan, S. (2000), *Reliability Assessment Using Stochastic Finite Element Analysis*. John Wiley & Sons, Inc, United States of America.

Hausler, E.A. and Koelling, M. (2004), "Performance of improved ground during the 2001 Nisqually earthquake", *Proceedings of the 5th International Conference on Case Histories in Geotechnical Engineering*, New York.

Hicks, M.A., Pisanò, F. and Peuchen, J. (2018), "Cone Penetration Testing 2018", *Proceedings of CPT'18, the 4th International Symposium on Cone Penetration Testing*, the Netherlands, London.

Idriss, I.M. and Boulanger, R.W. (2008), "Soil liquefaction during earthquakes: Monograph MNO-12, 261", Earthquake Engineering Research Institute, Oakland, California.

Ilbagitaher, S. and Alielahi, H. (2024), "Seismic fragility assessment of shored mechanically stabilized earth walls", *Geomech. Eng.*, **36**(3), 277-293. https://doi.org/10.12989/gae.2024.36.3.277.

Ishihara, K. (1985), "Stability of natural deposits during earthquakes", *Proceedings of 11th international conference on soil mechanics and foundation engineering*, San Francisco, CA, USA.

Iwasaki, T.F., Tatsuoka, K. and Yasuda, S.T. (1978), "A practical method for assessing soil liquefaction potential based on case studies at various sites in Japan", *Proceedings of the 2nd international conference on microzonation*, San Francisco, CA, USA.

Khanbabazadeh, H., Zulfikar, A.C. and Yesilyurt, A. (2020), "Basin edge effect on industrial structures damage pattern at clayey basins", *Geomech. Eng.*, **23**(6), 575-585. https://doi.org/10.12989/gae.2020.23.6.575.

Khoshnevisan, S., Juang, H., Zhou, Y.G. and Gong W. (2015), "Probabilistic assessment of liquefaction-induced lateral spreads using CPT—focusing on the 2010–2011 Canterbury earthquake sequence", *Eng. Geol.*, **192**, 113=128. https://doi.org/10.1016/j.enggeo.2015.04.001.

Kumar, S., Muley, P. and Madani, S.N. (2023), "Soil Liquefaction Potential of Kalyani Region, India", *Indian Geotech. J.*, **53**, 139-153. https://doi.org/10.1007/s40098-022-00658-4.

Lai, C.G., *et al*. (2021), "Technical guidelines for the assessment of earthquake-induce liquefaction hazard at urban scale", *Bull. Earthq. Eng.*, **19**(3), 4013–4057. https://doi.org/10.1007/s10518-020-00951-8.

Lee, D. H., Juang, C.H. and Ku, C.S. (2001), "Liquefaction performance of soils at the site of a partially completed ground improvement project during the 1999 Chi-Chi earthquake in Taiwan", *Can. Geotech. J.*, **38**(6), 1241-1253. https://doi.org/10.1139/t01-067.

Lee, D.H. and Lukas, R.G. (1995), "Geotechnical Engineering Circular No. 1 Dynamic Compaction", FHWA-SA-95-037; National Technical Information Servce, Springfield, Virginia 22161.

Maurer, B.W., Green, R.A. and Taylor, O.D.S. (2015), "Moving towards an improved index for assessing liquefaction hazard: Lessons from historical data", *Soils Found.*, **55**(4), 778-787. https://doi.org/10.1016/j.sandf.2015.06.010.

Meng, J.Y., Lu, D.G. and Shan, B.H. (2023), "Probabilistic-based seismic fragility assessment of earthquake-induced site liquefaction", *Soil Dyn. Earthq. Eng.*, **175**(108250), 1-12. https://doi.org/10.1016/j.soildyn.2023.108250.

Meslem, A., Iversen, H., Iranpour, K. and Lang, D. (2021), "A computational platform to assess liquefaction-induced loss at critical infrastructures scale", *Bull. Earthq. Eng.*, **19**(11), 4083-4114. https://doi.org/10.1007/s10518-020-01021-9.

Michalowski, R.L. and Nadukuru, S.S. (2012), "Static fatigue, time effects, and delayed increase in penetration resistance after dynamic compaction of sands", *J. Geotech. Geoenviron. Eng.*, **138**(5), 564–574. https://doi.org/10.1061/(ASCE)GT.1943-5606.0000611.

Moss, R.E.S., Seed, R.B., Kayen, R.E., Stewart, J.P., Der Kiureghian, A. and Cetin, K.O. (2006), "CPT-based probabilistic and deterministic assessment of in situ seismic soil liquefaction potential", *J. Geotech. Geoenviron. Eng.*, **132**(8), 1032-1051. https://doi.org/10.1061/(ASCE)1090-0241(2006)132:8(1032).

New Zealand geotechnical society (2016), Earthquake geotechnical engineering practice. Module 3: identification, assessment and mitigation of liquefaction hazard, New Zealand Geotechnical Society (NZGS) and Ministry of Business Innovation and Employment (MBIE), New Zealand.

OCDI (2020), Technical Standards and Commentaries for Port and Harbor Facilities in Japan, The Overseas Coastal Area Development Institute of Japan, Tokyo, Japan.

PIANC (2001), Seismic Design Guidelines for Port Structures, International Navigation Association, Balkema Publications, Tokyo, Japan.

Porter, K. (2021), A Beginner's Guide to Fragility, Vulnerability, and Risk. University of Colorado Boulder", University of Colorado Boulder and SPA Risk LLC, Denver CO, USA.

Rabeti Moghadam, M., Alielahi, H. and Sadeghi Abdollahi, A. (2017), "Numerical evaluation of liquefaction-induced damages in composite breakwaters and its application for performance-based improvement design", *Mar. Georesour. Geotec.*, **35**, 376-

396. https://doi.org/10.1080/1064119X.2016.1190428.
Robertson, P.K. and Wride, C.E. (1998), "Evaluating cyclic liquefaction potential using cone penetration test", *Can. Geotech. J.*, **35**(3), 442-459. https://doi.org/10.1139/t98-017.
Seed, H.B., Tokimatsu, K., Harder, L.F. and Chung, R.M. (1985), "Influence of SPT procedures in soil liquefaction resistance evaluations", *J. Geotech. Eng.*, **111**(12), 1425-1445. https://doi.org/10.1061/(ASCE)0733-9410(1985)111:12(1425).
Seed, H.B. and Idriss, I.M. (1971), "Simplified procedure for evaluating soil liquefaction potential", *J. Soil Mech. Found. Division*, **93**, 1249-1273.
Shen, M., Juang, C.H., Ku, C.S. and Khoshnevisan, S. (2019a), "Assessing effect of dynamic compaction on liquefaction potential using statistical methods – a case study", *Georisk Assessment and Management of Risk for Engineered Systems and Geohazards*, **13**(97), 1749-9526. https://doi.org/10.1080/17499518.2019.1623407.
Shen, M., Juang, C.H. and Chen, Q. (2019b), "Mitigation of liquefaction hazard by dynamic compaction - a random field perspective", *Can. Geotech. J.*, **56**, 1803-1815. dx.doi.org/10.1139/cgj-2018-0502.
Shenthan, T., Nashed, R., Thevanayagam, S. and Martin, G.R. (2004), "Liquefaction mitigation in silty soils using composite stone columns and dynamic compaction", *Earthq*. *Eng. Eng. Vib.n*, **3**(1), 39-50. https://doi.org/10.1007/BF02668849.
Sonmez, H. (2003), "Modification of the liquefaction potential index and liquefaction severity mapping for a liquefaction-prone area (Inegol, Turkey)", *Environ. Earth Sci.*, **44(**7), 862-871. https://doi.org/10.1007/s00254-003-0831-0.
Sonmezer, Y.B. and Korkmaz, E. (2023), "Estimation of the soil liquefaction potential through the Krill Herd algorithm", *Geomech. Eng.*, **33**(5), 487-506. https://doi.org/10.12989/gae.2023.33.5.487.
Yang, H., Liua, Z. and Xiea, Y. (2023), "Probabilistic liquefaction assessment based on an in-situ state parameter considering soil spatial variability and various uncertainties", *KSCE J. Civil Eng.*, **27**(10):4228-4239. https://doi.org/10.1007/s12205-023-0144-7.
Zheng, K., Wang, C., Zhao, Y., Bi, J. and Liu, H. (2023), "Theoretical and experimental exploration on the combined mode I + III fracture toughness of shale using the edge-notched disk bending method with acoustic emission monitoring", *Theor. Appl. Fract. Mech.*, **125**(103870). https://doi.org/10.1016/j.tafmec.2023.103870.

GC

Nomenclature

a_{max}: maximum horizontal acceleration (m/s²)
g: gravitational acceleration (9.81 m/s²)
σ_v: total vertical overburden stress at the respective depth (kPa)
σ'_{vo}: effective vertical overburden stress at the respective depth (kPa)
r_d: shear stress reduction factor
MSF: magnitude scaling factor
K_σ: overburden correction factor
M: seismic magnitude
Z: soil depth (m)
FC: percentage of soil fines
F_{sliq}: safety factor against liquefaction
H1*:* the thickness of the non-liquefied layer (m)
D: effective depth of compaction (m)
W: the weight of a compactor (ton)
H: the height of dropping weights (m)
n: empirical coefficient
AE: applied energy (KJ/m^2)
N: number of drops at each specific drop point location
P: number of passes
S: grid spacing (m^2)
ϕ: the standard cumulative distribution function
μ: median value of the distribution
σ: logarithmic standard deviation